TECHNICAL REPORT ARLCB-TR-79016

PRELIMINARY ANALYSIS OF A MANDREL FOR 105MM GUN TUBE FORGINGS

M. A. Hussain
S. L. Pu
J. D. Vasilakis

June 1979

US ARMY ARMAMENT RESEARCH AND DEVELOPMENT COMMAND
LARGE CALIBER WEAPON SYSTEMS LABORATORY
BENÉT WEAPONS LABORATORY
WATERVLIET, N. Y. 12189

AMCMS No. 3110.15.0003

PRON No. 32-6-P4941-01-M7-M7

DISCLAIMER

The findings in this report are not to be construed as an official Department of the Army position unless so designated by other authorized documents.

The use of trade name(s) and/or manufacturer(s) does not constitute an official indorsement or approval.

DISPOSITION

Destroy this report when it is no longer needed. Do not return it to the originator.

REPORT DOCUMENTATION PAGE

READ INSTRUCTIONS BEFORE COMPLETING FORM

1. REPORT NUMBER: ARLCB-TR-79016

2. GOVT ACCESSION NO.:

3. RECIPIENT'S CATALOG NUMBER:

4. TITLE (and Subtitle): PRELIMINARY ANALYSIS OF A MANDREL FOR 105MM GUN TUBE FORGINGS

5. TYPE OF REPORT & PERIOD COVERED:

6. PERFORMING ORG. REPORT NUMBER:

7. AUTHOR(s):
M. A. Hussain
S. L. Pu
J. D. Vasilakis

8. CONTRACT OR GRANT NUMBER(s):

9. PERFORMING ORGANIZATION NAME AND ADDRESS:
Benet Weapons Laboratory
Watervliet Arsenal, Watervliet, N.Y. 12189
DRDAR-LCB-TL

10. PROGRAM ELEMENT, PROJECT, TASK AREA & WORK UNIT NUMBERS:
AMCMS No. 3110.15.0003
PRON No. 32-6-P4941-01-M7-M7

11. CONTROLLING OFFICE NAME AND ADDRESS:
US Army Armament Research and Development Command
Large Caliber Weapon System Laboratory
Dover, New Jersey 07801

12. REPORT DATE: June 1979

13. NUMBER OF PAGES: 36

14. MONITORING AGENCY NAME & ADDRESS (if different from Controlling Office):

15. SECURITY CLASS. (of this report): UNCLASSIFIED

15a. DECLASSIFICATION/DOWNGRADING SCHEDULE:

16. DISTRIBUTION STATEMENT (of this Report)

Approved for public release; distribution unlimited.

17. DISTRIBUTION STATEMENT (of the abstract entered in Block 20, if different from Report)

18. SUPPLEMENTARY NOTES

19. KEY WORDS (Continue on reverse side if necessary and identify by block number)

Crack Analysis
Fatigue Analysis
Radial Forge
Thermal Stress

20. ABSTRACT (Continue on reverse side if necessary and identify by block number)

A simplified stress analysis of a mandrel used in rotary forging of 105mm M68 gun tube forgings is presented. High tensile stress occurs at the inner bore during a fraction of a forging cycle when two hammers are engaged with the billet. The combination of the tensile stresses due to mechanical and thermal loading is responsible for the fracture of the mandrel.

Assuming a semi-circular crack initiated at the inner bore of the mandrel and propagated in the radial direction, the stress intensity factors are

Continued from Block 20

computed based on the penny shaped crack under arbitrary loading. The remaining life of a mandrel having a semi-circular crack of 0.003 inch is predicted based on the most severe loading conditions and using the propagation equation for gun steel.

The effect of the reduction of the inner diameter of the mandrel on the mandrel life is studied. A four-fold life increase is predicted if the bore diameter is reduced from 1.969 to 1.4 inches. The effect of autofrettage is also studied. The mandrel life can be increased as much as 48 times if the mandrel is overstrained 50 percent.

TABLE OF CONTENTS

ILLUSTRATIONS

NOMENCLATURE

a	Bore radius of a mandrel, present design a = 0.9845".
b	Outside radius of a mandrel, present design b = 1.795".
c	Radius of a semi-circular crack; also the depth of a frontal crack.
E,G	Modulus of elasticity in tension and in shear respectively.
h	Uniform radial stress transferred to the contact region of the mandrel **h** = 38 Ksi used in this report to non-dimensionalize other stresses.
k	Thermal conductivity of steel.
K_1	Stress intensity factors of mode I.
r,θ	Cylindrical coordinate.
R	Ratio of b/a.
Sx	Compressive stress in the x-direction.
T	Temperature, T_a temperature at r = a.
u	Displacement.
α_o	$(1-2\nu)/(2-2\nu)$.
α,β	Coefficients in linear approximation of tangential stress.
η	One-half of the angle of contact between the mandrel and the tube.
ν	Poisson's ratio.
ρ	Ratio of a/b, ρ = 1/R, for the present design $\rho \approx 0.55$.
σ	Normal stress.
τ	Shear stress.

Φ, Φ_n	n = 0, 1, ...n, stress functions.
$\Phi_r, \Phi_\theta, \Phi_{r\theta}$	Partial derivatives $\partial\Phi/\partial r$, $\partial\Phi/\partial\theta$, $\partial^2\Phi/\partial r\partial\theta$.
ω	Percentage of autofrettage.

INTRODUCTION

In this report we present a simplified stress analysis of a mandrel used in the rotary forge process for 105mm gun tubes. The objective was to investigate the conditions of mandrel failures and the effects of various design parameters to enhance the life of such mandrels.

Essentially, there are three zones in the forging process, namely sinking, forging and sizing zones (Figure 1). Due to physical constraints, the sizing zone is subjected to higher stresses[1], and for our preliminary analysis, we shall consider this zone under the plane condition, i.e. independent of the axial dimension.

To study the crack propagation, it is necessary to consider the most severe loading configuration. Based on the design of the forging process, it seems that only two hammers are engaged with the preform during a fraction of the forging cycle, causing peak stresses in the mandrel.

Due to this non-axisymmetric loading for a fraction of the cycle, it is shown that there are regions of separation between the mandrel and the preform causing high tensile stresses at the inner radius of the mandrel.

Assuming a total load transfer to the mandrel through the contact region, the stresses are computed. Results compare favorably with a finite element method.

---

[1]Lahoti, G. D. and Altan, R., "Analysis and Optimization of the Radial Forging Process for Manufacturing Gun Barrels," WVT-CR-74054, 1974.

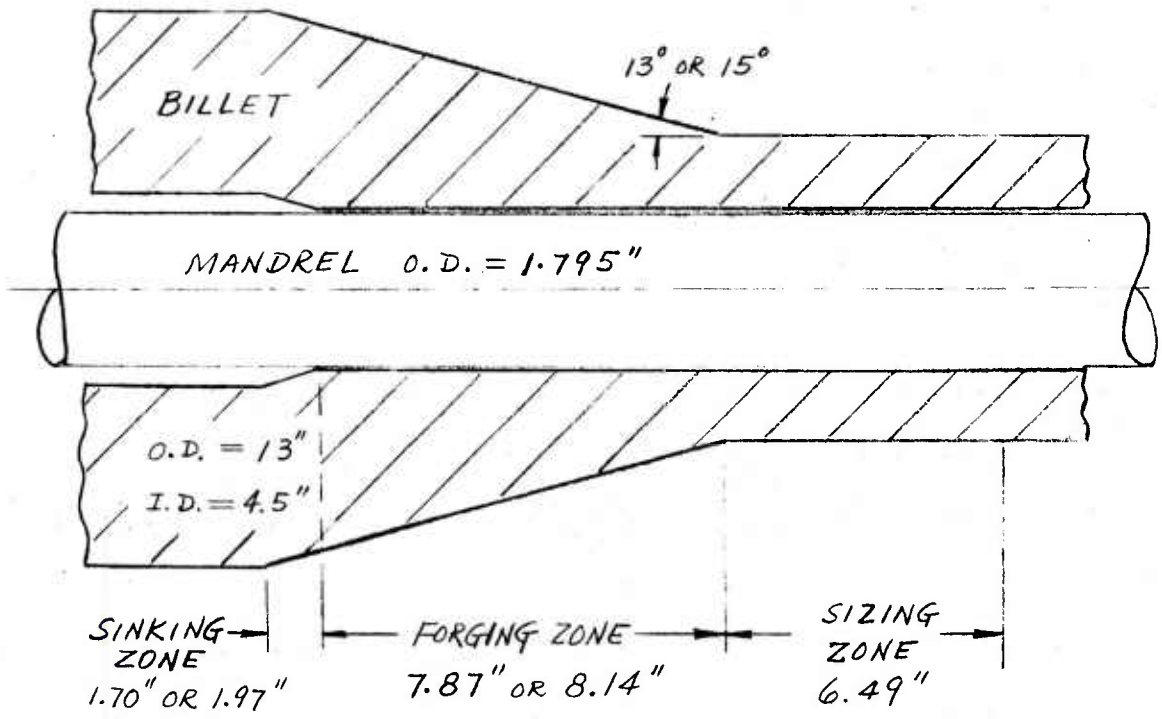

Figure 1. A schematic diagram of a mandrel and a billet showing sinking, forging and sizing zones.

Thermal analysis is carried out based on steady state conditions and known heat flux of the cooling fluid through the mandrel. These stresses are superposed with the mechanical stresses.

The stress intensity factors are then computed, based on the penny shaped crack under arbitrary loading conditions and they are compared with two dimensional frontal crack solutions.

The effects of change in the internal diameters of the mandrel and the effects of mandrel autofrettage are studied. An optimum percentage of autofrettage is obtained.

LOSS OF CONTACT

Consider a smooth unbonded inclusion as shown in Figure 2. Assume that the inclusion has a higher elastic modulus compared with the surrounding unbounded medium which is subjected to compressive stresses as shown.

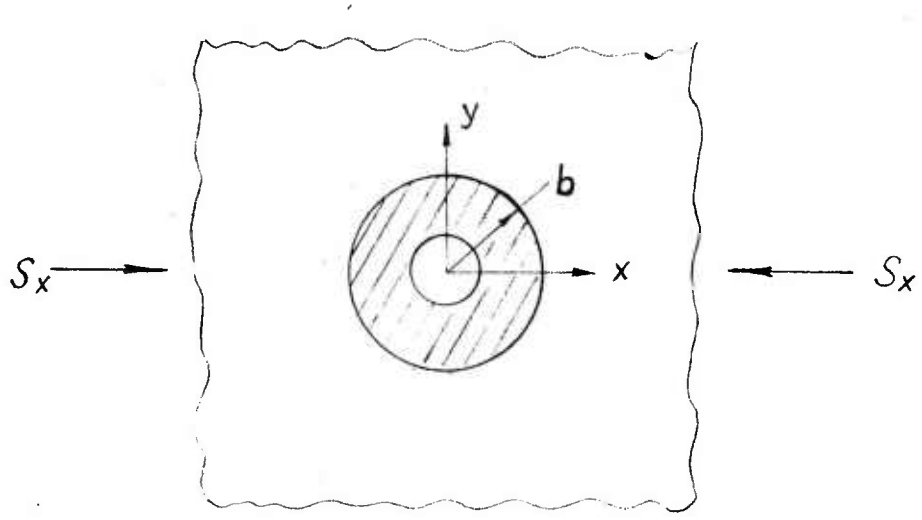

Figure 2. A mandrel surrounded by an infinite medium under a compressive stress, Sx.

Using the usual notations[2] the stress functions for the exterior medium can be written as

$$\Phi = -\frac{1}{4} Sxr^2 + \frac{1}{4} Sxr^2\cos 2\theta + A\log r + Dr^{-2}\cos 2\theta + F\cos 2\theta \qquad (1)$$

Using the boundary conditions of no shear stress and no radial displacement at the interface r = b, we have

$$A = -\frac{Sx}{2}(1-2\nu)b^2, \quad D = \frac{(1-2\nu)b^4 Sx}{4(5-6\nu)}, \quad F = \frac{b^2 Sx}{2(5-6\nu)}$$

The normal stress at the interface then becomes

$$\sigma_r = \frac{-Sx}{(5-6\nu)}\{(1-\nu)(5-6\nu) + 2(4-3\nu)\cos 2\theta\} \qquad (2)$$

From (2), it is easily seen that normal stresses have a transition from a compression to a tension at about $\theta = 53°$ for $\nu = 1/4$. Since the inclusion is unbonded, this shows the existence of separations at the interface. To determine this contact region, we have to reformulate the problem as done in the sequel.

[2]Timoshenko, S. and Goodier, J. N., THEORY OF ELASTICITY, 2nd Edition, McGraw-Hill, 1951.

FORMULATION OF CONTACT PROBLEM

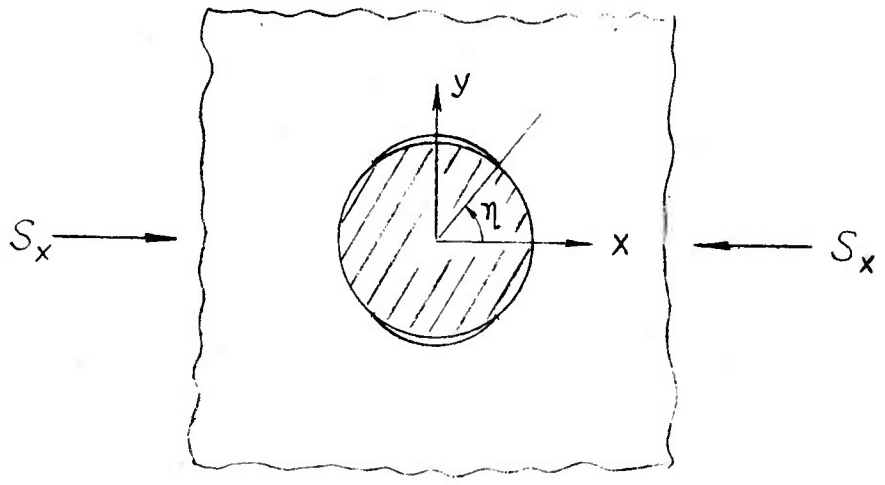

Figure 3. An unbonded inclusion in an infinite medium subjected to Sx showing regions of separation and regions of contact.

We reconsider the problem with contact regions and separation regions as shown in Figure 3. The stress functions are given by

$$\Phi = -\frac{1}{4} Sxr^2 + \frac{1}{4} Sxr^2\cos 2\theta + A_o \log r + \sum_{n=2,4}^{\infty} A_n r^{-n}\cos n\theta + \sum_{n=2,4}^{\infty} B_n r^{-n+2}\cos n\theta \qquad (3)$$

Boundary conditions are

$$\tau_{r\theta}(b,\theta) = 0 \qquad 0 \leq \theta \leq \pi/2 \qquad (4)$$

$$u_r(b,\theta) = 0 \qquad 0 \leq \theta < \eta \qquad (5)$$

$$\sigma_r(b,\theta) = 0 \qquad \eta < \theta \leq \pi/2 \qquad (6)$$

From (4), we have

$$B_2/b^2 = \frac{1}{4} Sx - 3 \frac{A_2}{b^4}$$

$$B_n = - \frac{(n+1)}{(n-1)} \frac{1}{b^2} A_n, \quad n>2 \tag{7}$$

From boundary conditions (6) and (5) using (7), we obtain

$$\frac{1}{2} E_o + \sum_{n=2,4,}^{\infty} E_n \cos n\theta = 0, \quad \eta>\theta\geq\pi/2 \tag{8}$$

$$K_1' E_o + \sum_{n=2,4,}^{\infty} K_n' E_n \cos n\theta = - \frac{Sx}{2} (1+2\cos 2\theta), \quad 0\leq\theta<\eta \tag{9}$$

where

$$\frac{1}{2} E_o = - \frac{1}{2} Sx + \frac{A_o}{b^2}$$

$$E_2 = - \frac{3}{2} Sx + \frac{6A_2}{b^4}$$

$$E_n = \frac{\alpha(n+1)A_n}{b^{n+2}}$$

$$K_1' = \frac{1}{4(1-\nu)} \quad , \quad K_2' = \frac{1}{6} \frac{(5-6\nu)}{(1-\nu)}$$

$$K_n' = \frac{n+\alpha_o}{n^2-1} \quad , \quad \alpha_o = \frac{1-2\nu}{2(1-\nu)}$$

Equations (8) and (9) are the dual series relation for the determination of the unknown contact area as well as unknown contact stresses.

SOLUTION OF DUAL SERIES AND THE CONTACT ANGLE

The dual series can be solved by iteration procedure after reducing to an integral equation. In this section we outline the solution procedure up to the second iteration. Using the asymptotic behavior of K_n' for large n, the dual series can be written as

$$\frac{1}{2}E_o + \sum_{n=2,4} E_n \cos n\theta = 0 \qquad \eta < \theta \leq \pi/2 \tag{10}$$

$$K_1' E_o + \sum_{2,4,6}^{\infty} \frac{1}{n} E_n \cos n\theta = -\frac{Sx}{2}(1+2\cos 2\theta) - \sum_{\substack{n=2,4 \\ 0 \leq \theta < \eta}}^{\infty} (K_n' - \frac{1}{n}) E_n \cos n\theta \tag{11}$$

Let

$$\frac{1}{2}E_o + \sum_{n=2,4}^{\infty} E_n \cos n\theta = H(\theta) \qquad 0 \leq \theta < \eta \tag{12}$$

hence

$$E_n = \frac{4}{\pi}\int_o^{\eta} H(t)\cos nt\,dt \tag{13}$$

Substituting E_n from (13) into (11) and by truncating the series on the right hand side up to n = 2, we get the following integral equation

$$K_1' \frac{4}{\pi}\int_o^{\eta} H(t)dt + \frac{4}{\pi}\int_o^{\eta} K(t,\theta)H(t)dt = -\frac{Sx}{2}(1+2\cos 2\theta) - (K_2' - \frac{1}{2})E_2 \cos 2\theta \tag{14}$$

Where the kernel is

$$K(t,\theta) = -\frac{1}{4}\log 2\left|\cos 2\theta - \cos 2t\right| \tag{15}$$

The above singular integral equation can be solved exactly, and the procedure can be repeated for any higher order approximation. The results of the solution are given in the following table

Poisson's ratio ν	0.2	0.3	0.4
Contact angle η	54.28°	49.31°	44.64°

The contact angle for the mandrel is about 50°. This is very close to the results we obtained in the previous section by a simpler model.

STRESS DISTRIBUTION IN THE MANDREL

Because of the dimensions involved the model analyzed in the previous section can be used for actual mandrel-preform contact. In addition, it is seen that the contact is independent of the magnitude of the load. Hence, even though more exact distribution of contact stresses may be parabolic, we may consider a uniform and complete load transfer from the hammer to the mandrel, see Figure 4. This assumption can be justified on the viscous flow model usually assumed in the metal forming process[3].

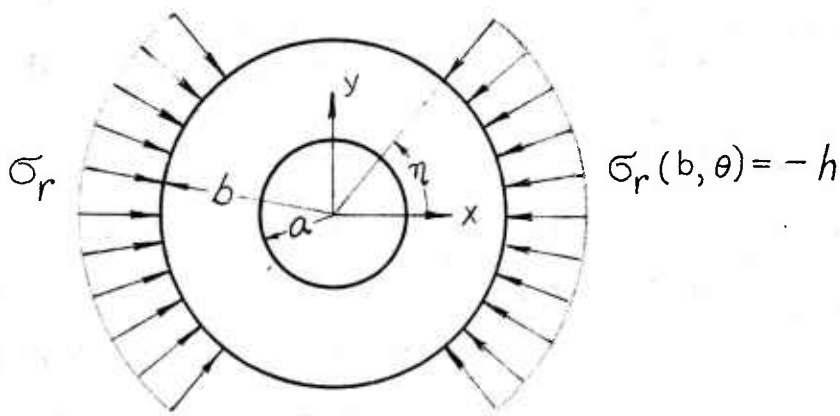

Figure 4. A mandrel is subjected to a uniform compressive stress over a part of the outer boundary.

[3]Nadai, A., THEORY OF FLOW AND FRACTURE OF SOLIDS, 2nd Edition, McGraw-Hill, 1950.

With the given dimensions supplied, this stress h is computed as 38 Ksi corresponding to a load per hammer of 700 tons with an allowance of 10% overload. Actual stress distribution will be non-dimensionalized with respect to this stress.

The stress function for the mandrel can be written as

$$\Phi = B_o \log r + D_o r^2 + \sum_{n=2,4}^{\infty} \{ \frac{A_n}{n-1} r^n + \frac{B_n}{n+1} r^{-n} + \frac{C_n}{n+1} r^{n+2} + \frac{D_n}{n-1} r^{-n+2} \} \cos n\theta \tag{16}$$

Boundary conditions are

$$\tau_{r\theta}(b,\theta) = 0 \qquad 0 \leq \theta \leq \pi/2 \tag{17}$$

$$\tau_{r\theta}(a,\theta) = 0 \qquad 0 \leq \theta \leq \pi/2 \tag{18}$$

$$\sigma_r(a,\theta) = 0 \qquad 0 \leq \theta \leq \pi/2 \tag{19}$$

$$\sigma_r(b,\theta) = \begin{cases} -h & 0 \leq \theta < \eta \\ 0 & \eta < \theta \leq \pi/2 \end{cases} \tag{20}$$

From (17) and (18), with $\rho = \frac{a}{b} = \frac{1}{R}$, we have

$$C_n = -A_n a^{-2} \frac{(R^{2n-2}-1)}{(R^{2n}-1)} - B_n a^{-2n-2} \frac{(R^2-1)}{R^2(R^{2n}-1)} \tag{21}$$

$$D_n = A_n a^{2n-2} R^{2n-2} \frac{(R^2-1)}{(R^{2n}-1)} - B_n a^{-2} \frac{(R^{2n+2}-1)}{R^2(R^{2n}-1)} \tag{22}$$

And from (19), we obtain

$$B_n = \frac{[(n+1)R^{2n} - nR^{2n-2} - 1]R^2 a^{2n}}{(R^{2n+2} + (n-1)R^2 - n)} A_n \tag{23}$$

For convenience, let us define the following quantities

$$\begin{aligned}
\Gamma_1 &= -(1-\rho^{2n-2})/(1-\rho^{2n}) \\
\Gamma_2 &= \rho^{-2}(1-\rho^2)/(1-\rho^{2n}) \\
\Gamma_3 &= \rho^{2n}(\rho^{-2}-1)/(1-\rho^{2n}) \\
\Gamma_4 &= \rho^{-2}(1-\rho^{2n+2})/(1-\rho^{2n}) \\
\Gamma_5 &= \rho^{2n}(-\rho^{2n}-n\rho^2+n+1)/[-n\rho^{2n+2}+(n-1)\rho^{2n}+1] \\
\Gamma_6 &= \rho^2(\Gamma_1-\Gamma_2\Gamma_5) \\
\Gamma_7 &= \rho^{-2n+2}(\Gamma_3-\Gamma_4\Gamma_5) \\
\Gamma_8 &= -n\rho^{-n+2}(1+\Gamma_5)-(n-2)\rho^{-n}\Gamma_6-(n+2)\rho^n\Gamma_7
\end{aligned} \tag{24}$$

Using (21), (22), (23) and (24), it is seen that

$$\sigma_r(b,\theta) = B_o\left(\frac{1}{b^2} - \frac{1}{a^2}\right) + \sum_{n=2,4}^{\infty} A_n a^{n-2}\Gamma_8 \cos n\theta \tag{25}$$

From (20), using Fourier inversion formula, we have

$$\begin{aligned}
B_o &= -\frac{2h\eta}{\pi}\frac{a^2b^2}{(a^2-b^2)} \\
A_n a^{n-2} &= -\frac{4h}{\pi n}\frac{\sin n\eta}{\Gamma_8}
\end{aligned} \tag{26}$$

This formally completes the problem. The stress distribution of interest to us is the tangential stress. It is given by

$$-\frac{\sigma_\theta}{h} = \frac{2\eta}{\pi}\frac{\rho^2}{(1-\rho^2)}\left(\frac{1}{\rho^2}+\frac{b^2}{r^2}\right) + \sum_{n=2,4}^{\infty}\frac{4\sin n\eta}{n\pi\Gamma_8}\{n\rho^{-n+2}\left(\frac{r}{b}\right)^{n-2} +$$

$$n\rho^{-n+2}\left(\frac{r}{b}\right)^{-n-2}\Gamma_5 + (n+2)\rho^{-n}\left(\frac{r}{b}\right)^n\Gamma_6 + (n-2)\rho^n\left(\frac{r}{b}\right)^{-n}\Gamma_7\}\cos n\theta \tag{27}$$

For the dimensions of the mandrel, the above stress distributions for $\theta = 0$ and $\theta = \pi/2$ are plotted in Figure 5. A similar finite element model was constructed and shown in Figure 6 and the results for the finite element model are also indicated in Figure 5.

THERMAL STRESSES IN THE MANDREL

Due to lack of temperature data for the mandrel, several heat transfer models have been tried and ruled out because of unreasonable high thermal stresses. The final model used in our computation is a simple one dimensional, steady state heat flow method. The temperatures of the coolant, water, in and out the mandrel are measured, and the capacity of the water pump is known. This gives the heat flux taken away by the coolant which is balanced by the heat flux transferred from the preform to the mandrel. The temperature gradient $\frac{dT}{dr}$ at the mandrel preform interface is then obtained.

The heat balance is given by

$$k \frac{dT}{dr} (2\pi b)\ell = \text{heat flux taken away by the coolant}$$

Using measurements recorded in an actual manufacturing run of M68 tube in the rotary forge: the inlet and outlet temperatures of cooling water are 65°F and 80°F, the flow is 80 gallons per minute; taking the thermal conductivity k = 0.11 cal/°C-min-sec, ℓ = 368 mm, we obtain

$$\left.\frac{dT}{dr}\right|_{r=b} = 3.625 \quad °C/mm \tag{28}$$

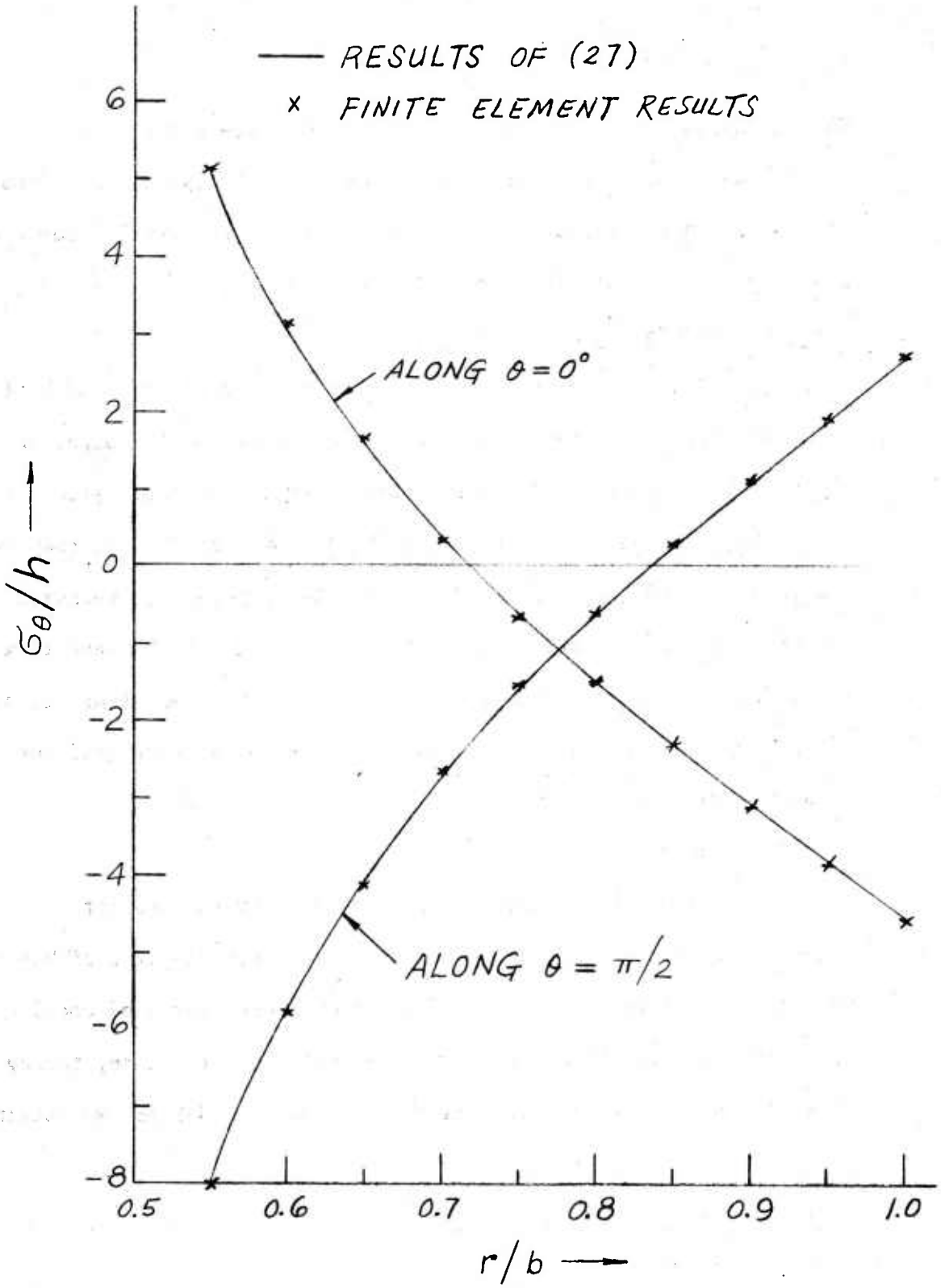

Figure 5. Non-dimensional stresses as a function of r/b for θ = 0 and π/2 for the mandrel shown in Figure 4.

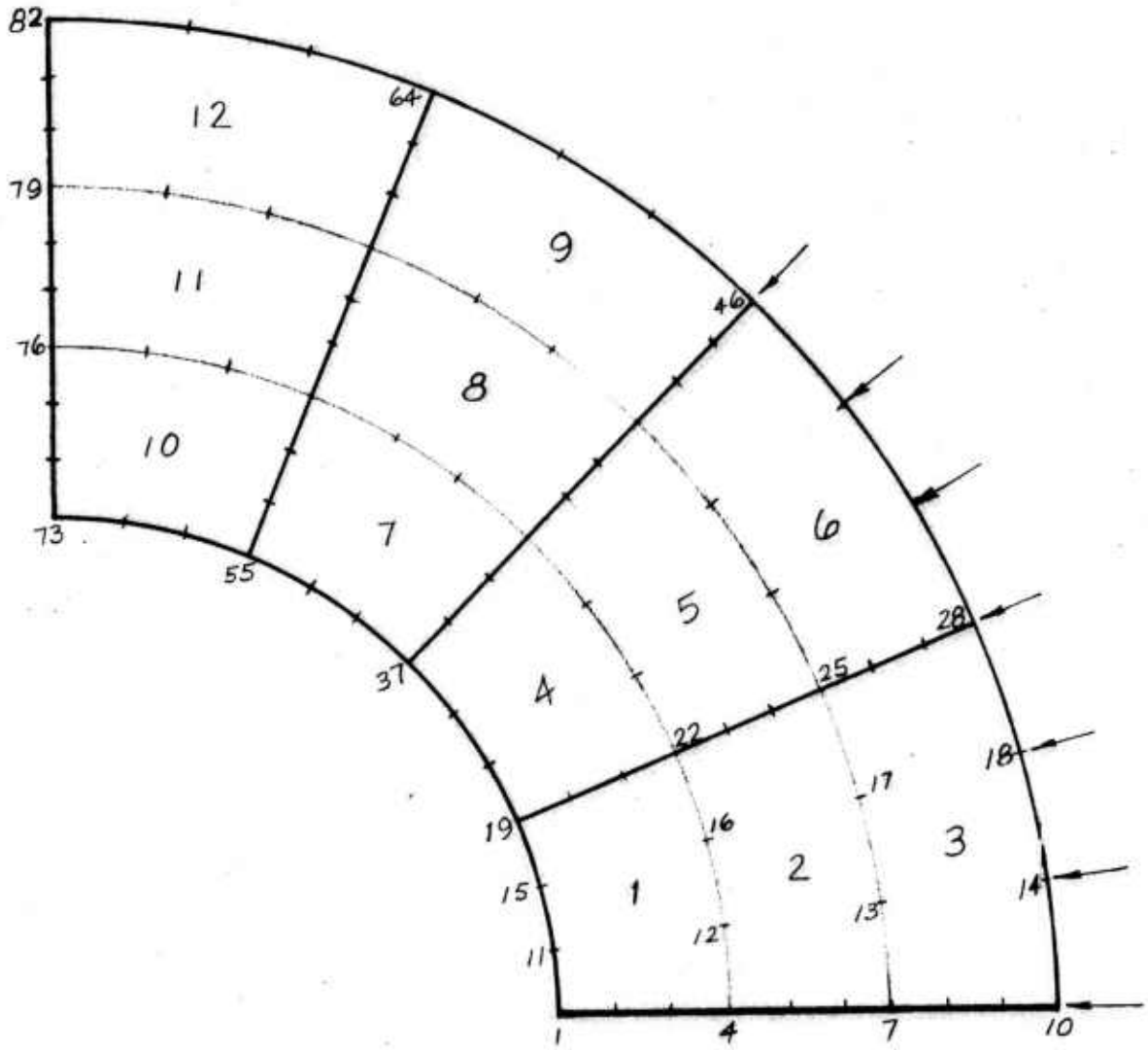

Figure 6. A finite element idealization of one quarter of the mandrel shown in Figure 4.

Assume a steady state condition

$$T = c_1 \log r + c_2 \tag{29}$$

Using the boundary conditions (28) and $T_a = 80°F$, we have

$$\begin{aligned} T_b - T_a &= 165.27 \log(1/\rho) \ , \quad °C \\ &= 297.49 \log(1/\rho) \ , \quad °F \end{aligned} \tag{30}$$

Defining parameters δ and s as

$$\delta = \frac{E\alpha(T_b - T_a)}{2(1-\nu)\log(1/\rho)}$$

$$s = \frac{\rho^2 \log(1/\rho)}{(1-\rho^2)} \tag{31}$$

The thermal stress, normalized with respect to h, is given by

$$\frac{\sigma_\theta}{h} = \frac{\delta}{h}\left\{-1-\log(r/b)+s\left(1 + \frac{1}{(r/b)^2}\right)\right\} \tag{32}$$

where δ/h for the mandrel is 1.17.

TOTAL STRESS DISTRIBUTION AND STRESS INTENSITY FACTORS

The total stress distribution for the mandrel is the sum of mechanical and thermal stresses. From (27) and (32), we have

$$\left(\frac{\sigma_\theta}{h}\right)_{\text{total}} = \left(\frac{\sigma_\theta}{h}\right)_{\text{mechanical}} + \left(\frac{\sigma_\theta}{h}\right)_{\text{thermal}} \tag{33}$$

It should be noted that this distribution of stress is valid only for a fraction of a complete forging cycle when only two hammers are being engaged. For the rest of the cycle when all four hammers are engaged the stress distribution may not be as severe. However there exists a prolonged thermal load. For the present design the tangential stress at $\theta = 0$ (under the hammer) is plotted in Figure 7.

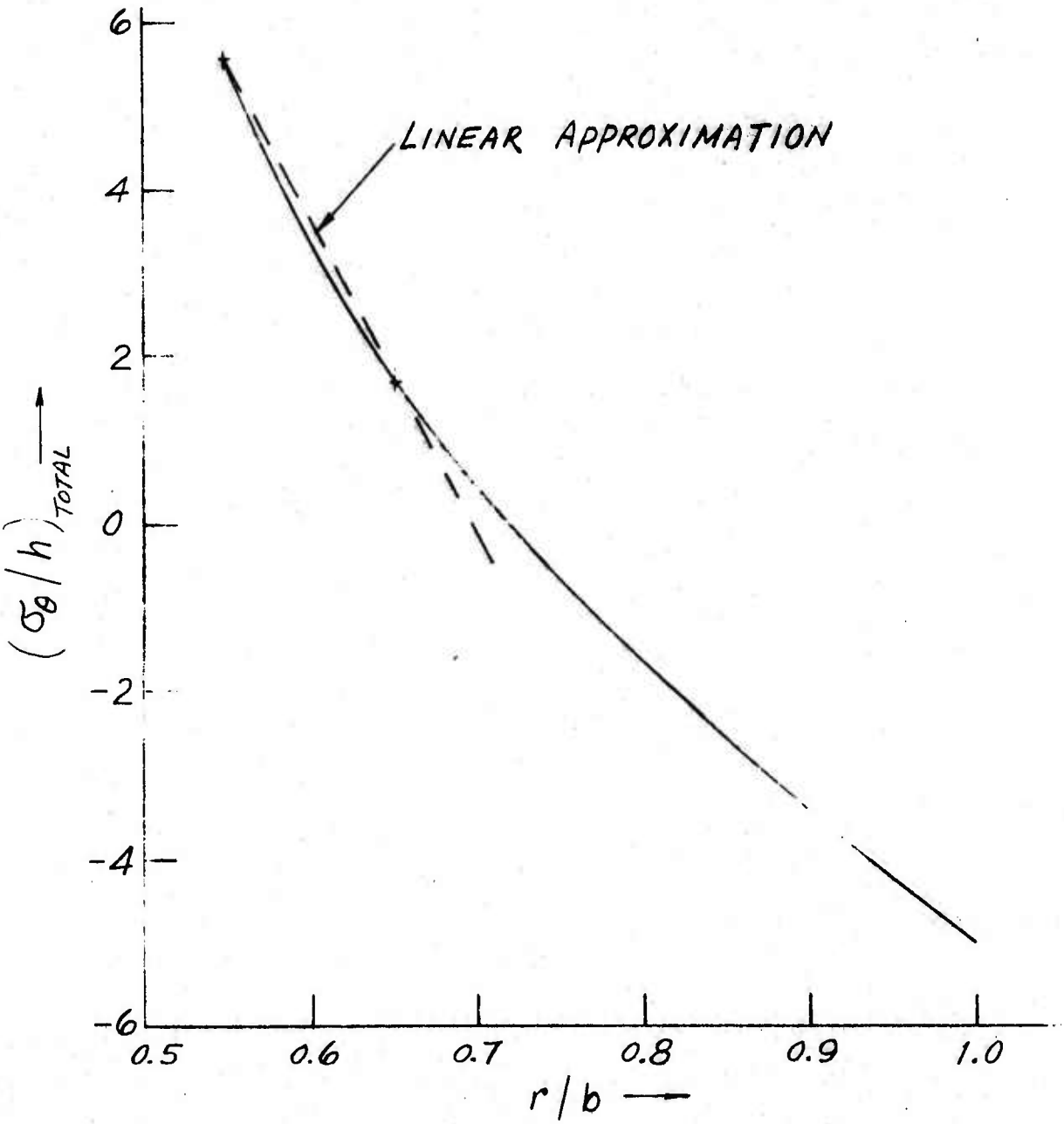

Figure 7. The total tangential stress distribution along $\theta = 0$ and its linear approximation near the bore of the mandrel.

For the determination of stress intensity factors, we approximate the stress distribution by a linear one in the neighborhood of the inside radius as shown by the dotted line in Figure 7.

As far as the stress intensity factor is concerned, we consider a penny shaped crack of radius c under uniform and linear stress distributions. For the solution of the problem, we use Boussinesq-Papkovitch functions and reduce the problem to the one function approach given in Ref. [4].

$$
\begin{aligned}
2Gu_r &= (1-2\nu)\Phi_r + z\Phi_{rz} \\
2Gu_\theta &= (1-2\nu)\frac{1}{r}\Phi_\theta + \frac{z}{r}\Phi_{\theta z} \\
2Gu_z &= -2(1-\nu)\Phi_z + z\Phi_{zz} \\
\sigma_r &= (1-2\nu)\Phi_{rr} + z\Phi_{zrr} - 2\nu\Phi_{zz} \\
\sigma_\theta &= -(1-2\nu)\Phi_{rr} - \Phi_{zz} + \frac{z}{r}\Phi_{rz} + \frac{z}{r^2}\Phi_{z\theta\theta} \\
\sigma_z &= -\Phi_{zz} + z\Phi_{zzz} \\
\tau_{r\theta} &= \frac{(1-2\nu)}{r}\Phi_{r\theta} - \frac{(1-2\nu)}{r^2}\Phi_\theta + \frac{z}{r}\Phi_{r\theta z} - \frac{z}{r^2}\Phi_{\theta z} \\
\tau_{rz} &= z\Phi_{rzz} \\
\tau_{z\theta} &= \frac{z}{r}\Phi_{\theta zz}
\end{aligned}
\tag{34}
$$

where

$$\nabla^2\Phi = 0 \tag{35}$$

---

[4] Green, A. E. and Zerne, W., THEORETICAL ELASTICITY, 2nd Edition, Oxford, 1968.

For the problem at hand, we use Kobayashi Potentials[5] as

$$\Phi_n = A_n \cos n\theta \int_0^\infty K^{-3/2} J_{n+3/2}(Kc) J_n(Kr) e^{-Kz} dK \tag{36}$$

Using (34) and (36) after some manipulation, it can be shown

$$2Gu_z(z=0) = \begin{cases} 0 & , \quad r>c \\ 2(1-\nu) \dfrac{(c^2-r^2)^{1/2}\, r^n}{\sqrt{2}\, c^{n+3/2}\Gamma(\frac{3}{2})} A_n \cos n\theta & , \quad r \leq c \end{cases} \tag{37}$$

$$\sigma_z(z=0) = \begin{cases} \dfrac{\sqrt{2}\, c^{n-1/2}(r^2-c^2)^{-1/2} A_n}{r^n \Gamma(\frac{1}{2})} - \dfrac{(2n+1) c^{n-1/2} A_n}{\sqrt{2\pi}(n+\frac{1}{2}) r^{n+1}} F(\tfrac{1}{2};\ n+\tfrac{1}{2};\ n+\tfrac{3}{2},\ \dfrac{c^2}{r^2}), & r>c \\ -\dfrac{(2n+1)\Gamma(n+1/2)}{\Gamma(n+1)\sqrt{2}\, c^{n+3/2}} A_n r^n \cos n\theta & , \quad r<c \end{cases} \tag{38}$$

The reason for selecting the potential given in (36) becomes clear if we study (37) and (38). It is seen that the stress has the crack singularity at r = c and the displacement vanishes outside of r = c. These are precisely the conditions required for a penny shaped crack under normal stress of the form $r^n \cos n\theta$.

For our purpose, it is sufficient to consider only the two-term approximation, i.e. $\Phi = \Phi_0 + \Phi_1$ where Φ_0, Φ_1 are given by n = 0,1 in (36);

$$\sigma_z(z=0) = \alpha + \beta \frac{x}{b} = \alpha + \beta(\frac{r}{b})\cos\theta \tag{39}$$

---

[5] Sneddon, I. N., MIXED BOUNDARY VALUE PROBLEMS IN POTENTIAL THEORY, John Wiley & Sons, 1966.

Using (38), we have

$$A_0 = \sqrt{\frac{2}{\pi}}\,\alpha\, c^{3/2}$$
$$A_1 = \frac{2}{3}\sqrt{\frac{2}{\pi}}\,\beta\, c^{5/2} \tag{40}$$

From the definition of stress intensity factors, we have

$$K_1 = \frac{\sqrt{2}}{c}\,(A_0+A_1) \tag{41}$$

It is known that for a semi-circular surface flaw, the stress intensity factor at the deepest end of the crack very closely approximates the stress intensity factor for penny shaped crack in an unbounded medium provided the load distribution is similar. Hence, to a very good approximation, we take σ_z in equation (39) to represent a linear approximation of $(\sigma_\theta)_{total}$ of (33). The result for the present mandrel design (a = 0.9845") of such computations is shown in Figure 8. It is seen that the critical crack size of the semi-circular shape is about 20 thousandths of an inch for a fracture toughness of 30 Ksi$\sqrt{in}$. Even though the cracks at failure seem to be of the semi-circular shape, we computed the stress intensity factor for a frontal crack by a similar analysis, i.e.

$$K_1 = \sqrt{\pi c}\,\{\sigma_1 F_1(\frac{c}{b-a}) + \sigma_2 F_2(\frac{c}{b-a})\} \tag{42}$$

where σ_1 and σ_2 correspond to uniform tension and bending stresses, respectively, in the linear approximation of $(\sigma_\theta)_{total}$, and F_1 and F_2 are given by Ref. [6],

---

[6]Tada, H., Paris, P., and Irwin, G., THE STRESS ANALYSIS OF CRACKS HANDBOOK, Del Research Corp., 1973.

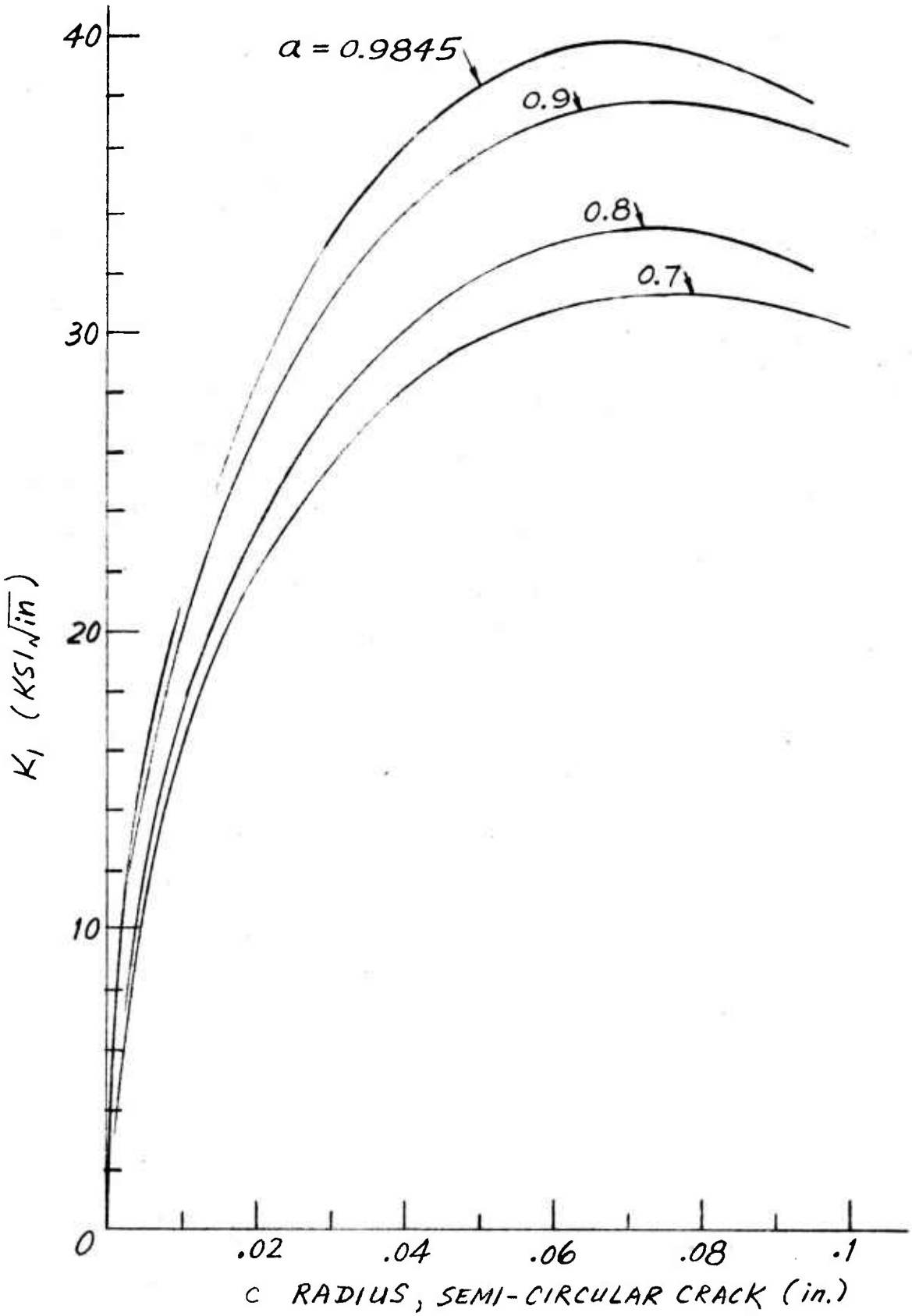

Figure 8. Stress intensity factors as a function of c for various values of the bore radius a of the mandrel.

$$F_1(x) = 1.12 - 0.231x + 10.55x^2 - 21.72x^3 + 30.39x^4$$
$$F_2(x) = 1.122 - 1.4x + 7.33x^2 - 13.08x^3 + 14.0x^4 \quad (43)$$

The results are shown in Figure 9. It can be seen from Figures 8 and 9 that the stress intensity factors are much higher for frontal cracks for the same c.

EFFECT OF VARIATION OF THE INNER RADIUS OF THE MANDREL

Similar analysis was carried out by fixing the outer radius of the mandrel and varying the inner radius. The outer radius was fixed due to the design constraint, and the total heat flux was assumed the same even with a slight reduction in the inner radius.

The total stress at $\theta = 0$ was computed for each value of inner radii and the non-dimensionalized results are shown in Figure 10. It is seen that the maximum tensile stress at the bore can be reduced by 30% for the inner diameter a = 1.4 inch. The corresponding stress intensity factors are shown in Figure 8. It can be seen that the critical crack size is now increased by 150% for the same inner radius of a = 1.4".

At this point, it is worhtwhile to compare the number of remaining cycles the mandrel can sustain this load without a catastrophic fracture. Assuming an undetactable crack of 0.003" and using the propagation equation for gun steel, approximate results are given below. In the table, 1600 cycles is used to obtain the number of tubes from the number of cycles.

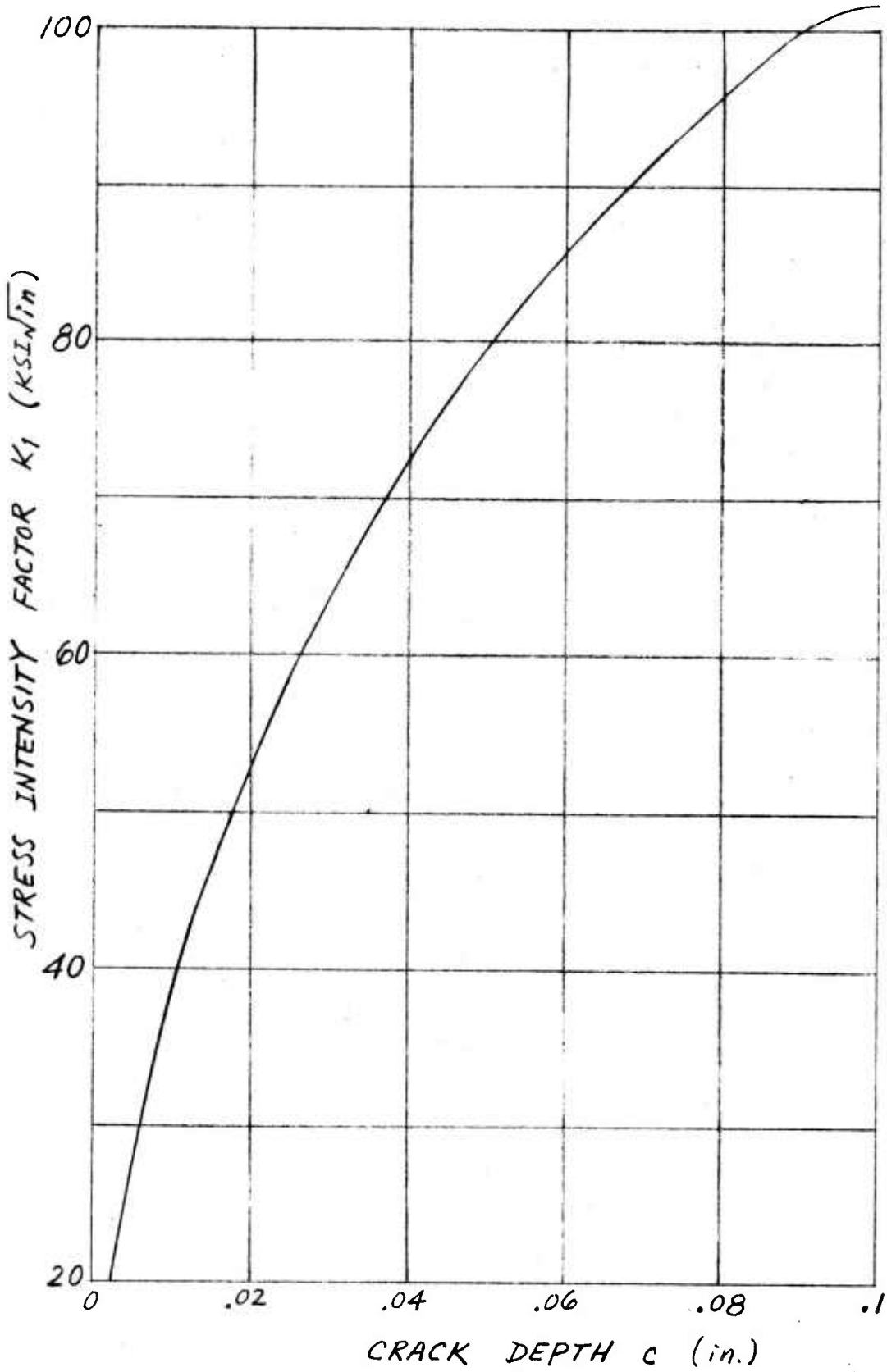

Figure 9. Stress intensity factors as a function of the depth c of a frontal crack.

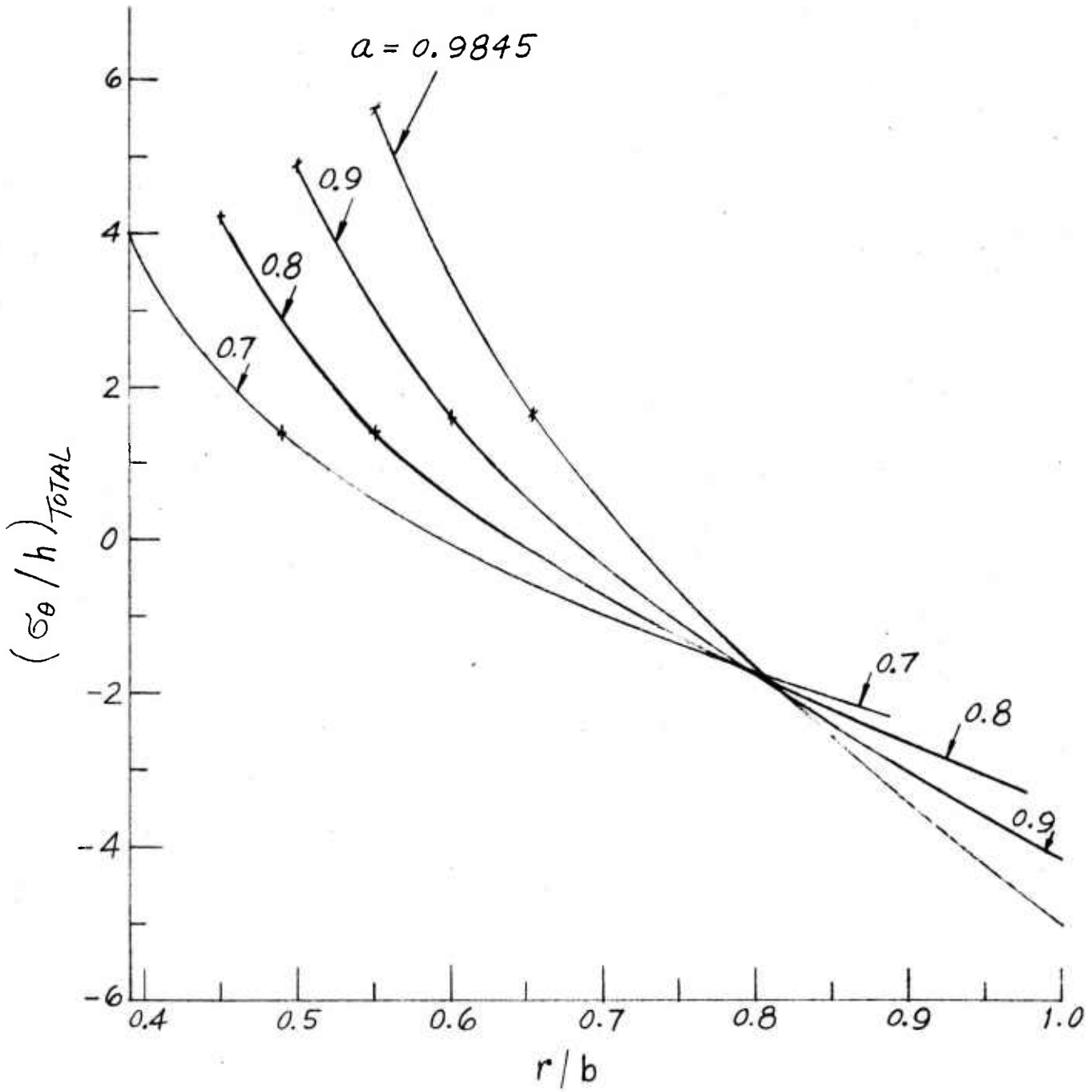

Figure 10. The total tangential stress distribution along $\theta = 0^\circ$ for various bore sizes of the mandrel.

Inner Radius a inch	Remaining Life to Failure		Ratio of Mandrel Life
	In Cycles	In No. of Tubes	
0.9845	3530	2	1
0.9	6580	4	2
0.8	10880	7	3.5
0.7	13350	8	4

This table shows that by changing the inner diameter from 1.969" to 1.4", there is a four-fold increase in the life of the mandrel. Actual life may be longer than those indicated in the table because of our assumption of worst conditions during each cycle.

EFFECT OF MANDREL AUTOFRETTAGE

An examination of Figure 7 indicates that the stress distribution is exactly the opposite of the residual stress distribution of a fully autofrettaged tube. This suggests the beneficial effect of having autofrettaged mandrels.

Let ω be the percentage of autofrettage, the residual stress is

$$(\sigma_\theta)_{residue} = \frac{\sigma_y}{\sqrt{3}} \{2\log \frac{r}{\omega} + 1 + \frac{\omega^2}{b^2} - \frac{\frac{a^2}{b^2} + \frac{a^2}{r^2}}{1 - \frac{a^2}{b^2}} (2\log \frac{\omega}{a} + 1 - \frac{\omega^2}{b^2})\} \qquad a<r<\omega \qquad (44)$$

Thus from (44) and (33), we obtain the total stresses and the results are plotted in Figure 11, showing a dramatic reduction in tensile stresses.

The corresponding stress intensity factors are shown in Figure 12, again showing the dramatic decrease. As done previously, we compute the remaining life to failure and the results are tabulated in the

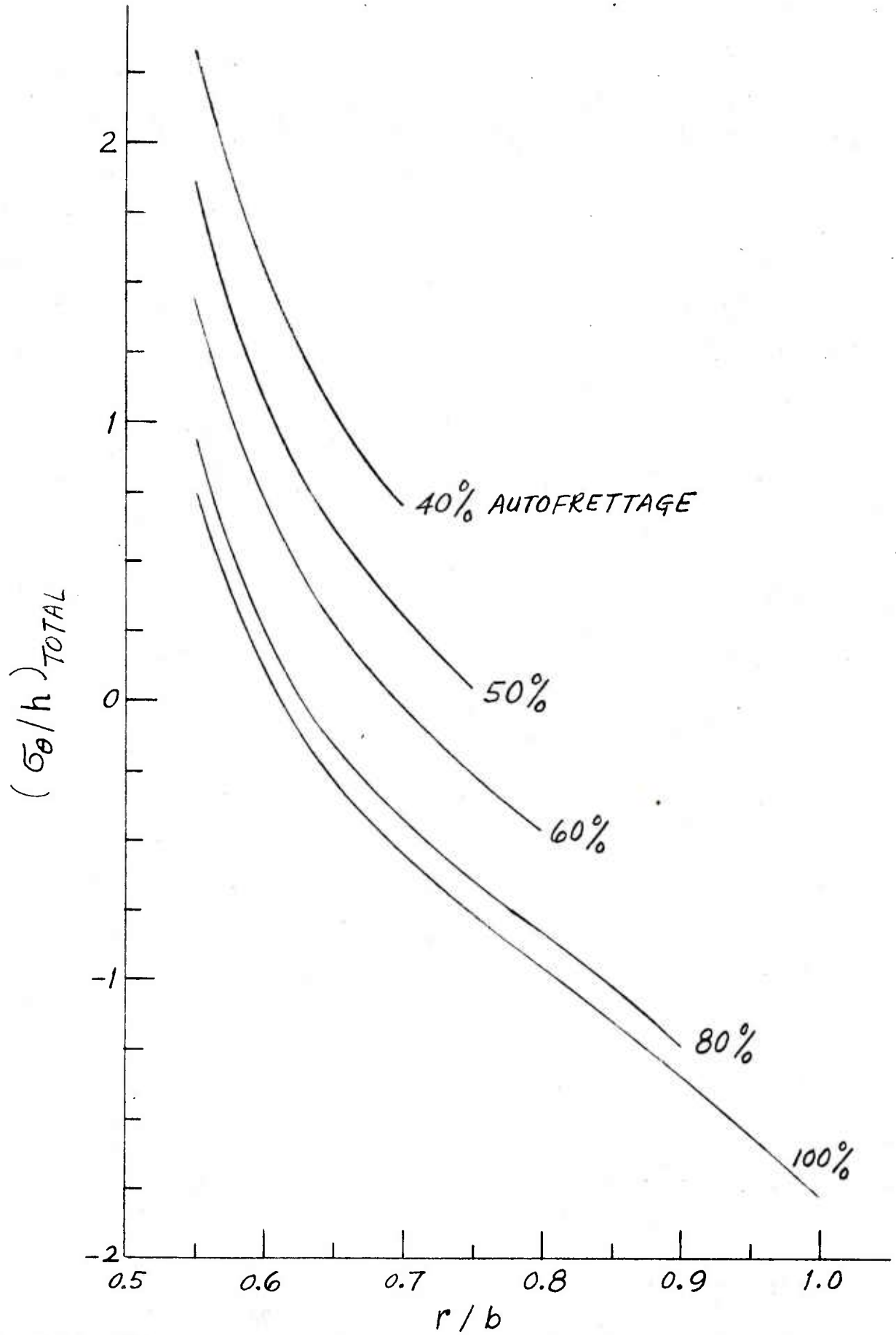

Figure 11. The total tangential stress distribution along θ = 0 for the mandrel of present design but with various percentages of autofrettage.

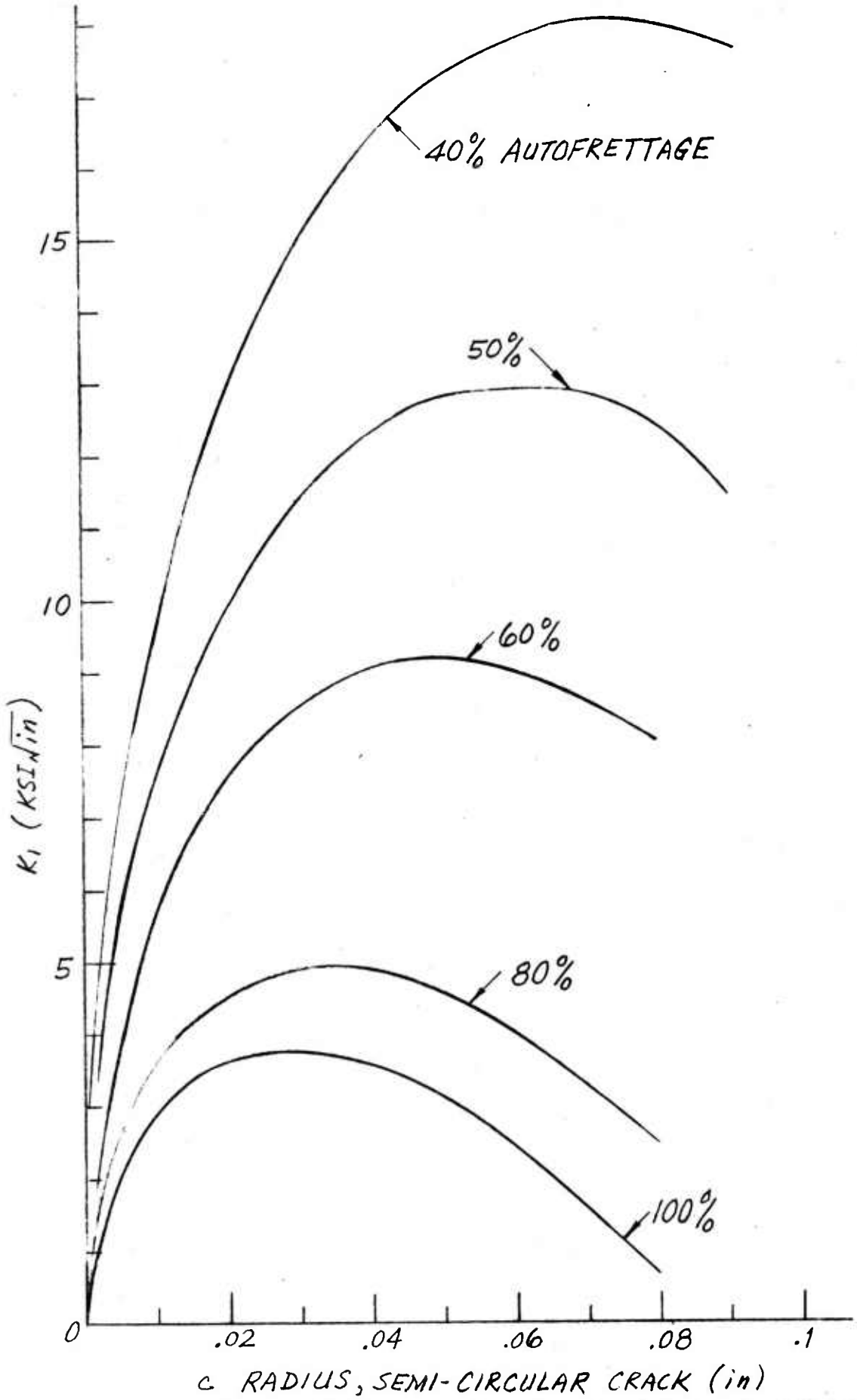

Figure 12. Stress intensity factors as a function of c for the mandrel of present design but with various percentages of autofrettage.

following table.

Percentage of Autofrettage ω	Remaining Life to Failure		Ratio of Mandrel Life
	In Cycles	In No. of Tubes	
0%	3530	2	1
40%	47770	29	15
50%	154000	96	48
60%	218000	136	68
80%	885000	554	277
100%	1660000	1040	520

The preceding table indicates a dramatic increase in the mandrel life. However, this was based on the analysis valid only for a fraction of a forging cycle. The rest of the cycle induces a large compressive stress at the inner bore. The sum of this compressive stress and the compressive stress due to atuofrettage may cause a reverse yielding phenomenon at the inner bore of the mandrel. Such an analysis was carried out and it was found that 50% autofrettage gives us the optimum value.

In Figure 13, we also plotted the stress distribution for a solid mandrel. This shows negligible stresses in the mandrel.

DISCUSSION

In this report we have done only a preliminary analysis in two dimensions. The proper analysis should include some three-dimensional effects and some non-linear effects. However, before such an extensive analysis is undertaken, it is necessary to apply proper boundary and working conditions. For example, proper temperature distribution

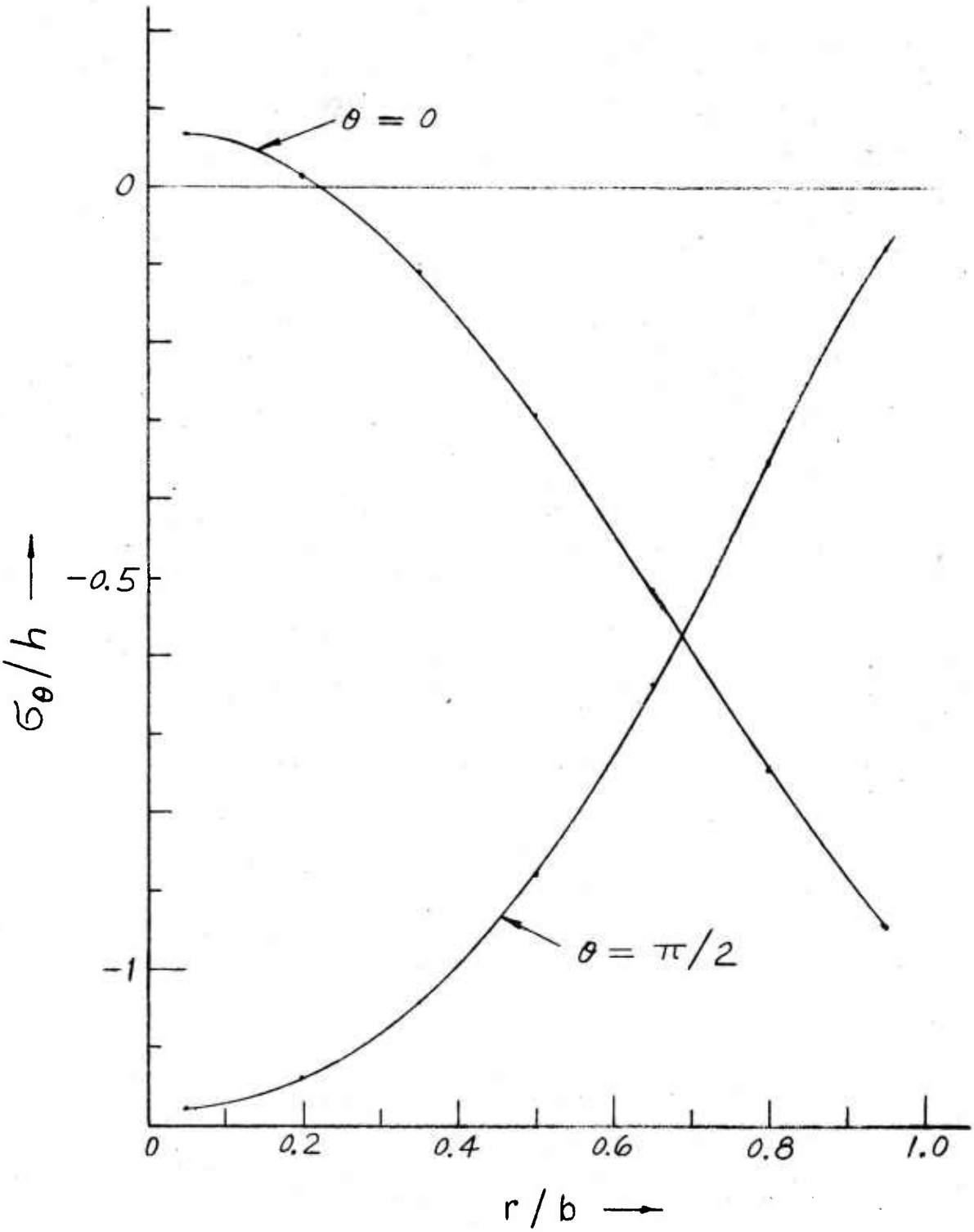

Figure 13. The tangential stresses as a function of r/b for θ = 0 and π/2 for a solid mandrel subjected to a loading shown in Figure 4 with η = 50°.

should be measured, exact amount of heat removed should be determined, and proper calibration of load per hammer, etc., should be given.

CONCLUSION

It is seen that by changing the inside diameter to 1.4", we increase the life of the mandrel by a factor of four. On the other hand, 40-50% autofrettage increases the life of the mandrel by a factor of 15-45. The computations were based on an initial crack length of 0.003". To further increase the life, cleaner material with higher fracture toughness should be used.

REFERENCES

1. Lahoti, G. D. and Altan, R., "Analysis and Optimization of the Radial Forging Process for Manufacturing Gun Barrels," WVT-CR-74054, 1974.
2. Timoshenko, S. and Goodier, J. N., THEORY OF ELASTICITY, 2nd Edition, McGraw-Hill, 1951.
3. Nadai, A., THEORY OF FLOW AND FRACTURE OF SOLIDS, 2nd Edition, McGraw-Hill, 1950.
4. Green, A. E. and Zerne, W., THEORETICAL ELASTICITY, 2nd Edition, Oxford, 1968.
5. Sneddon, I. N., MIXED BOUNDARY VALUE PROBLEMS IN POTENTIAL THEORY, John Wiley & Sons, 1966.
6. Tada, H., Paris, P., and Irwin, G., THE STRESS ANALYSIS OF CRACKS HANDBOOK, Del Research Corp., 1973.

WATERVLIET ARSENAL INTERNAL DISTRIBUTION LIST

	NO. OF COPIES
COMMANDER	1
DIRECTOR, BENET WEAPONS LABORATORY	1
CHIEF, DEVELOPMENT ENGINEERING BRANCH	1
ATTN: DRDAR-LCB-DA	1
-DM	1
-DP	1
-DR	1
-DS	1
-DC	1
CHIEF, ENGINEERING SUPPORT BRANCH	1
CHIEF, RESEARCH BRANCH	2
ATTN: DRDAR-LCB-RA	1
-RC	1
-RM	1
-RP	1
TECHNICAL LIBRARY	5
TECHNICAL PUBLICATIONS & EDITING UNIT	2
DIRECTOR, OPERATIONS DIRECTORATE	1
DIRECTOR, PROCUREMENT DIRECTORATE	1
DIRECTOR, PRODUCT ASSURANCE DIRECTORATE	1

NOTE: PLEASE NOTIFY DIRECTOR, BENET WEAPONS LABORATORY, ATTN: DRDAR-LCB-TL, OF ANY REQUIRED CHANGES.

EXTERNAL DISTRIBUTION LIST (CONT)

	NO. OF COPIES
COMMANDER US ARMY RESEARCH OFFICE P.O. BOX 1211 RESEARCH TRIANGLE PARK, NC 27709	1
COMMANDER US ARMY HARRY DIAMOND LAB ATTN: TECH LIB 2800 POWDER MILL ROAD ADELPHIA, MD 20783	1
DIRECTOR US ARMY INDUSTRIAL BASE ENG ACT ATTN: DRXPE-MT ROCK ISLAND, IL 61201	1
CHIEF, MATERIALS BRANCH US ARMY R&S GROUP, EUR BOX 65, FPO N.Y. 09510	1
COMMANDER NAVAL SURFACE WEAPONS CEN ATTN: CHIEF, MAT SCIENCE DIV DAHLGREN, VA 22448	1
DIRECTOR US NAVAL RESEARCH LAB ATTN: DIR, MECH DIV CODE 26-27 (DOC LIB) WASHINGTON, D.C. 20375	1 1
NASA SCIENTIFIC & TECH INFO FAC P.O. BOX 8757, ATTN: ACQ BR BALTIMORE/WASHINGTON INTL AIRPORT MARYLAND 21240	1

	NO. OF COPIES
COMMANDER DEFENSE DOCU CEN ATTN: DDC-TCA CAMERON STATION ALEXANDRIA, VA 22314	12
METALS & CERAMICS INFO CEN BATTELLE CCLUMBUS LAB 505 KING AVE COLUMBUS, OHIO 43201	1
MPDC 13919 W. BAY SHORE DR. TRAVERSE CITY, MI 49684	1
MATERIEL SYSTEMS ANALYSIS ACTV ATTN: DRXSY-MP ABERDEEN PROVING GROUND MARYLAND 21005	1

NOTE: PLEASE NOTIFY COMMANDER, ARRADCOM, ATTN: BENET WEAPONS LABORATORY, DRDAR-LCB-TL, WATERVLIET ARSENAL, WATERVLIET, N.Y. 12189, OF ANY REQUIRED CHANGES.

EXTERNAL DISTRIBUTION LIST

	NO. OF COPIES
ASST SEC OF THE ARMY RESEARCH & DEVELOPMENT ATTN: DEP FOR SCI & TECH THE PENTAGON WASHINGTON, D.C. 20315	1
COMMANDER US ARMY MAT DEV & READ. COMD ATTN: DRCDE 5001 EISENHOWER AVE ALEXANDRIA, VA 22333	1
COMMANDER US ARMY ARRADCOM ATTN: DRDAR-TSS DRDAR-LCA (PLASTICS TECH EVAL CEN) DOVER, NJ 07801	2 1
COMMANDER US ARMY ARRCOM ATTN: DRSAR-LEP-L ROCK ISLAND ARSENAL ROCK ISLAND, IL 61299	1
DIRECTOR US ARMY BALLISTIC RESEARCH LABORATORY ATTN: DRDAR-TSB-S (STINFO) ABERDEEN PROVING GROUND, MD 21005	1
COMMANDER US ARMY ELECTRONICS COMD ATTN: TECH LIB FT MONMOUTH, NJ 07703	1
COMMANDER US ARMY MOBILITY EQUIP R&D COMD ATTN: TECH LIB FT BELVOIR, VA 22060	1
COMMANDER US ARMY TANK-AUTMV R&D COMD ATTN: TECH LIB - DRDTA-UL MAT LAB - DRDTA-RK WARREN, MICHIGAN 48090	1 1
COMMANDER US MILITARY ACADEMY ATTN: CHMN, MECH ENGR DEPT WEST POINT, NY 10996	1
COMMANDER REDSTONE ARSENAL ATTN: DRSMI-RB DRSMI-RRS DRSMI-RSM ALABAMA 35809	2 1 1
COMMANDER ROCK ISLAND ARSENAL ATTN: SARRI-ENM (MAT SCI DIV) ROCK ISLAND, IL 61202	1
COMMANDER HQ, US ARMY AVN SCH ATTN: OFC OF THE LIBRARIAN FT RUCKER, ALABAMA 36362	1
COMMANDER US ARMY FGN SCIENCE & TECH CEN ATTN: DRXST-SD 220 7TH STREET, N.E. CHARLOTTESVILLE, VA 22901	1
COMMANDER US ARMY MATERIALS & MECHANICS RESEARCH CENTER ATTN: TECH LIB -DRXMR-PL WATERTOWN, MASS 02172	2

NOTE: PLEASE NOTIFY COMMANDER, ARRADCOM, ATTN: BENET WEAPONS LABORATORY, DRDAR-LCB-TL, WATERVLIET ARSENAL, WATERVLIET, N.Y. 12189, OF ANY REQUIRED CHANGES.